

# Failure analysis of hydrophilic and hydrophobic aerogels under liquid nitrogen thermal shock

Ai Du <sup>1,2,\*</sup>, Mingfang Liu <sup>1,2</sup>, Shangming Huang <sup>1,2</sup>, Conghang Li <sup>3</sup> and Bin Zhou <sup>1,2,\*</sup>

1. Shanghai Key Laboratory of Special Artificial Microstructure Materials and Technology, Tongji University, Shanghai 200092, P. R. China;

2. School of Physics Science and Engineering, Tongji University, Shanghai 200092, China;

3. Laboratory of Space Mechanical and Thermal Integrative Technology, Shanghai Institute of Satellite Engineering, Shanghai 200240, P. R. China.

Received: 15 April 2016; Accepted: 26 April 2016; Published: 2 May 2016

**Abstract:** As the best thermal insulator, aerogels could be used for high-efficiency insulation under exoplanet environment. There is the high day-night temperature difference in the exoplanets, thus the failure analysis of the aerogels under thermal shock could be studied. In this paper, hydrophilic and hydrophobic fiber-reinforced silica aerogels were forced to undergo liquid nitrogen-room temperature thermal shocks. Thermal conductivity, mechanical property and the microstructure were characterized for understanding the failure mechanism. It was found that after multiple shocks, the thermal conductivity of hydrophilic aerogel increased 35.5% after the first shock and kept in a high value, while that of the hydrophobic aerogel increased 19.5% and kept in a relatively low value. Pore size distribution results showed that after the first shock the peak pore size of the hydrophilic aerogel increased from 18 nm to 25 nm due to the shrinkage of the skeleton, while the peak pore size of the hydrophobic aerogel kept at ~9 nm probably induced by the spring-back effect. The high-strain hardening and low-strain soften behaviors further demonstrated the skeleton shrinkage of the hydrophilic aerogel. The existence of the free water in the infrared spectra of both aerogels indicated the driving force of the skeleton shrinkage may be the volume change of the absorbed water during freezing process. For further demonstrating the mechanism, the aerogels were treated at 80 °C under vacuum environment before conducting shock experiments. After the first shock, the thermal conductivities of the hydrophilic and hydrophobic aerogels were increased only 14.0% and 0.4%, respectively. In addition, multiple shock experiments showed that the failure processes of the hydrophilic and hydrophobic aerogels are irreversible and reversible, respectively, revealing their different failure modes.

**Keywords:** thermal shock, aerogel, hydrophilic, hydrophobic, failure, planet exploration

---

## 1. Introduction

Due to the hierarchical, multi-level and nanoporous microstructure and many unique properties, aerogel is different from ordinary materials and is even considered to be a new state of matter.[1]

Aerogel material, apart from high porosity, low bulk density, and high specific surface, possesses a very low thermal conductivity. [2, 3] as the most well-known and extensively studied aerogel, silica aerogel is treated as the ultralight insulation material, because it not only resists relatively high temperature fluctuation but also has endurance in harsh environments such as high temperature, low temperature or alternating temperature, etc. [4] Since it was first prepared by Kislter in 1931, silica aerogel had been applied in various fields especially in aerospace engineering. Silica aerogel was first used as the insulation materials in the exploration missions including Mars Rover, Sojourner and Pathfinder.

In particular, for Mars exploration, the landing site for the exoplanet planets has a surrounding temperature ranging from  $-130\text{ }^{\circ}\text{C}$  to  $30\text{ }^{\circ}\text{C}$ . And what's worse, this temperature may turn as low as to  $-150\text{ }^{\circ}\text{C}$ . Because of the great temperature variation, it is a great challenge for the materials to retain their heat resistance performance after the thermal shock from the dramatically varied temperature. [5, 6] Among these materials, aerogel with a nanoscale skeleton is one of the most sensitive materials which should be evaluated firstly.

As a promising material, fiber-reinforced silica aerogel has been used for the thermal insulation of the space shuttle liquid fuel, isolating the heat generated by the rocket, and ensure the spacecraft work normally after entering the high temperature or low temperature environment of all parts. NASA has conducted many astronomical missions by using this type aerogel as the thermal insulator. In this paper, we studied the failure analysis of the silica aerogels under liquid nitrogen thermal shock, which is simulating the environment of exoplanets. Two kinds of aerogels with the hydrophilic and hydrophobic surface were compared to study the different failure behaviors. Also, in order to avoid the influence of the liquid on the microstructure, the aerogels were covered with a plastic bag before immersing into the liquid nitrogen. The microstructure, thermal conductivity and mechanical property were evaluated during the shock processes.

## 2. Results

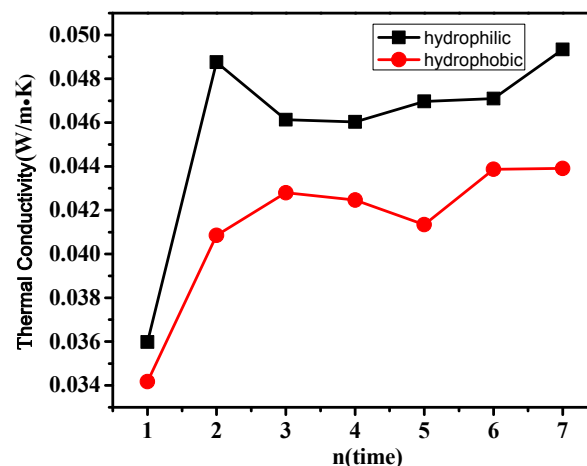


**Figure 1.** Thermal conductivity of the hydrophilic and hydrophobic aerogels changing with cycle times in air.

Fig 1 shows the thermal conductivity of hydrophilic and hydrophobic fiber-reinforced silica aerogels (Hereinafter referred to as hydrophilic and hydrophobic aerogels, respectively) under liquid nitrogen thermal shocks in the air. It indicates that the thermal conductivity of hydrophilic and hydrophobic aerogels increase under the first cycle of liquid nitrogen thermal shock by a large margin (from  $0.036\text{ W/(m}\cdot\text{K)}$  to  $0.049\text{ W/(m}\cdot\text{K)}$  for the hydrophilic aerogel and from  $0.034\text{ W/(m}\cdot\text{K)}$  to  $0.041\text{ W/(m}\cdot\text{K)}$  for the hydrophobic aerogel, respectively). The conductivity of the samples after the next

several cycles almost remain the same. The average values of the hydrophilic and hydrophobic aerogels are  $\sim 0.048$  W/(m·K) and  $\sim 0.043$  W/(m·K), respectively.

With the cycles increased, the thermal conductivity of samples was increased (Fig 1). It indicates that the microstructure of both samples may have changed under the liquid nitrogen shock. Thus the samples were tested by scanning electron microscope (SEM) in order to characterize their morphology evolutions.

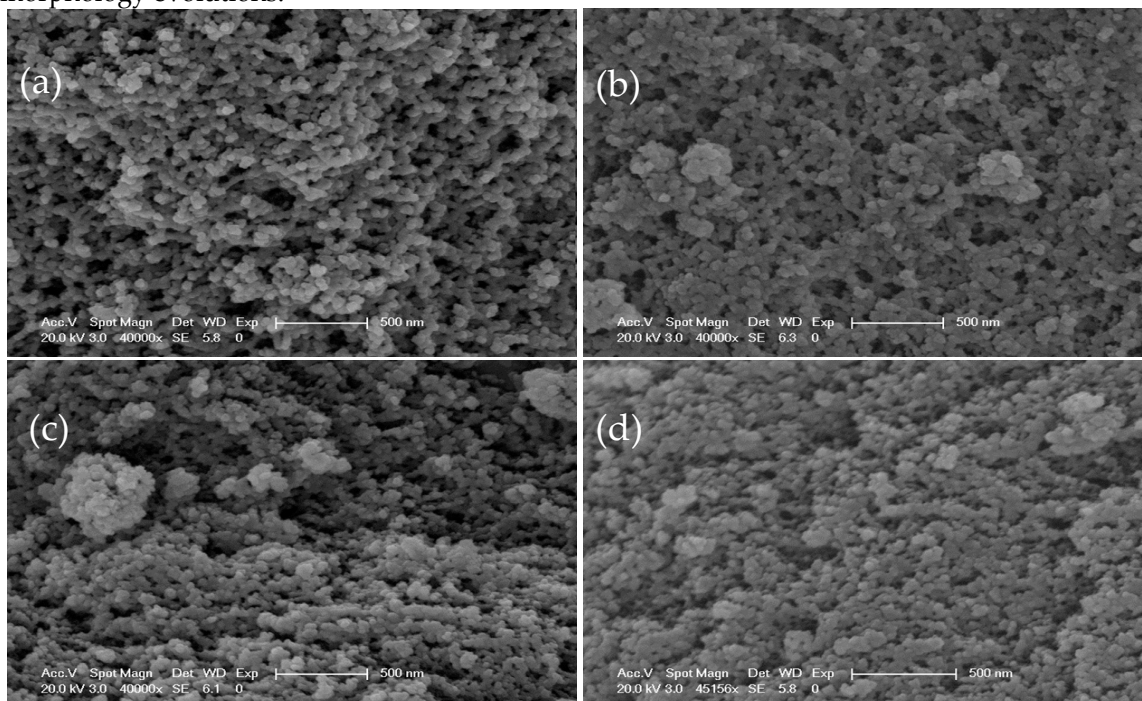
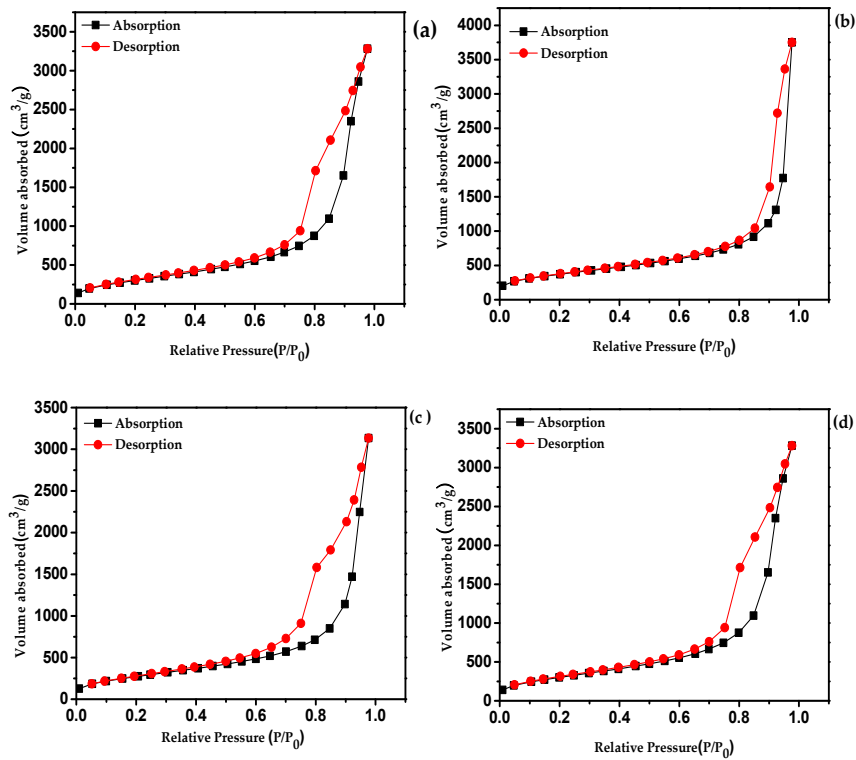


**Figure 2.** SEM image of hydrophilic aerogels before (a) and after (b) the first thermal shock and hydrophobic silica aerogels before (c) and after (d) the first thermal shock (Scale bar: 500 nm).

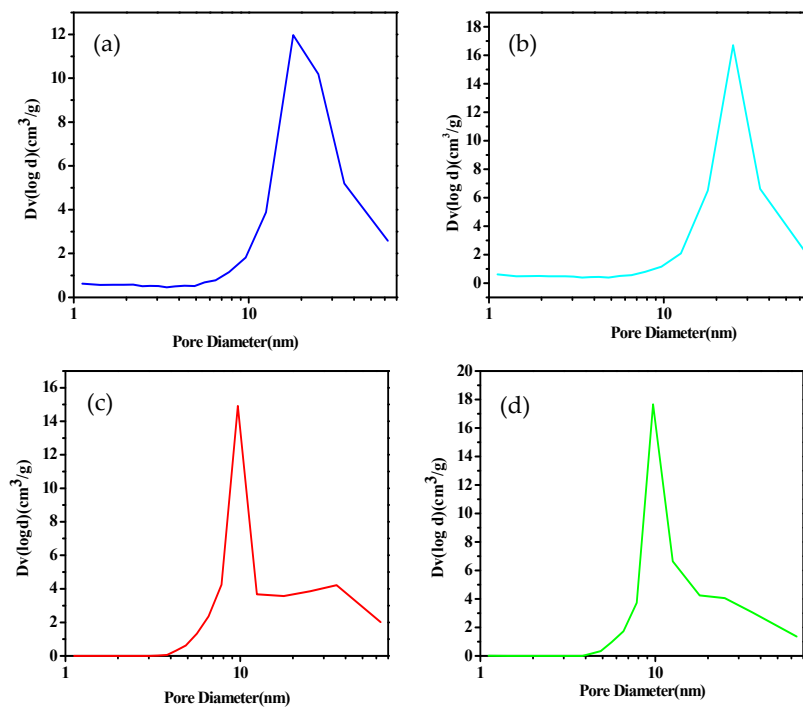
Fig 2 shows the microstructure of hydrophilic and hydrophobic aerogels before and after thermal shock. The SEM images indicated that the entire sample had highly porous networks, and aerogel particle is no obvious compact structure before shock in Fig 2a, while with the first thermal shock, hydrophilic aerogels tended to have a structure with larger pores and thicker skeletons (Fig2b). The pore size of hydrophilic aerogel seems to increase.

Figure 2c and figure 2d are respectively SEM images of hydrophobic silica aerogels before and after the first thermal shock. From the SEM images, it is clearly seen that, skeleton and pore size have no obvious change.

The specific surface areas and pore size distribution of both aerogel are further studied. The adsorption and desorption branches of the isotherms is analyzed by applying the Brunner-Emmet-Teller (BET) and Barrett-Joyner-Halenda (BJH) methods,[7] respectively. Relevant results are all list in Table 1. Fig 3 shows the Nitrogen adsorption and desorption isotherms.



**Figure 3.** Nitrogen adsorption (black-filled squares) and desorption isotherms of the hydrophilic aerogels before (a) and after (b) the first thermal shock, and the hydrophobic silica aerogels before (c) and after (d) the first thermal shock.



**Figure 4.** Pore size distribution of the hydrophilic aerogels before (a) and after (b) the first thermal shock, and the hydrophobic silica aerogels before (c) and after (d) the first thermal shock.

Sample	Specific surface area(m <sup>2</sup> /g)	Average pore size(nm)	Peak pore size(nm)	Pore volume (cm <sup>3</sup> /g)
a	1521	16.31	18	6.135
b	1316	17.67	25	5.814
c	1002	19.41	9	4.861
d	1117	18.22	9	5.087

**Table 1.** The specific surface area and pore structure parameters of the hydrophilic aerogels before (a) and after (b) the first thermal shock, and the hydrophobic silica aerogels before(c) and after (d) the first thermal shock.

parameters of the hydrophilic aerogels before (a) and after (b) the first thermal shock, and the hydrophobic silica aerogels before(c) and after (d) the first thermal shock.

As shown in Fig 4 and table 1, the peak pore size of the hydrophilic aerogel increased from 18 nm to 25 nm after the first shock, that indicates the skeleton becomes thicker and pore size turn into bigger, while the peak pore size of the hydrophobic aerogel kept at ~9 nm before and after thermal shock. Table 1 shows that specific surface area of hydrophilic aerogels change from 1521 m<sup>2</sup>/g to 1316 m<sup>2</sup>/g (Sample a, c), while specific surface area of hydrophobic aerogels increase from 1002 m<sup>2</sup>/g to 1117 m<sup>2</sup>/g (Sample b, d).

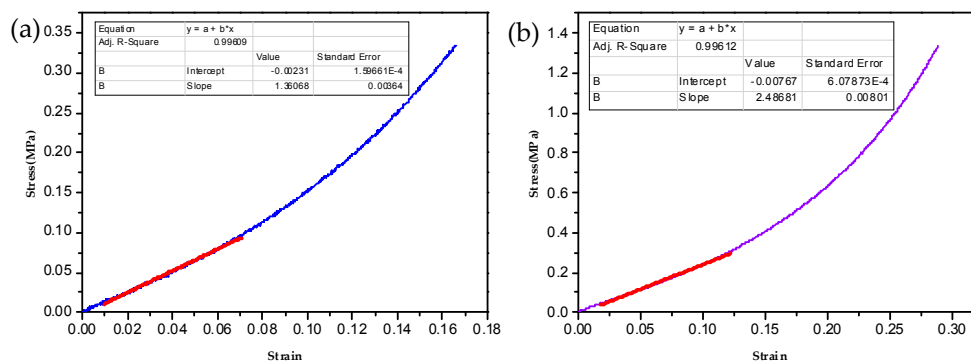


**Figure 5.** Stress-stain curve of the hydrophilic aerogels before (a) and after (b) the first thermal shock

Large change of hydrophilic aerogels microstructure prompted us to study the specific failure mechanism. We study two types of the mechanical properties with high strain and low strain (dynamic thermomechanical analysis, DMA) condition on the hydrophilic aerogels before and after the first thermal shock.

Stress-strain curve of hydrophilic aerogels are exhibited in Fig. 5(a) (b). The samples before and after thermal shock were compressed up to 16% and 28% of its original height, respectively. The porous structure can be deformed elastically at the beginning of the compression test and the slope in this range was used to calculate Young' modulus.[8] As provided in Fig 5, for hydrophilic aerogels, the slope of sample after thermal shock is 2.487 MPa while the slope of sample before thermal shock is 1.361 MPa.

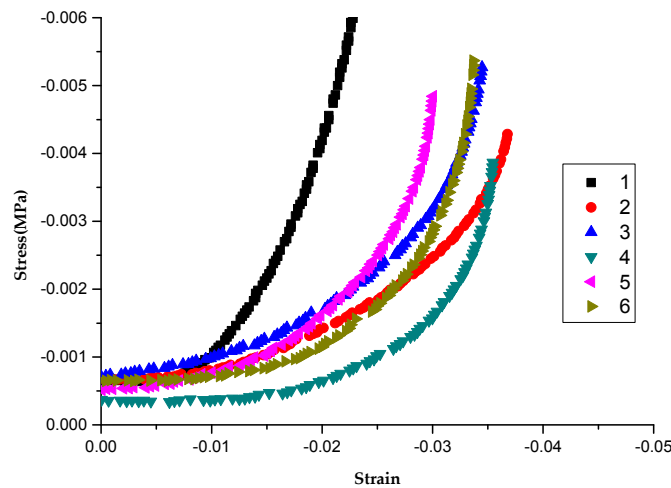


**Figure 6.** Low-strain spring-back compression testing results of hydrophilic fiber-reinforced silica aerogels along with the cycles of thermal shock.

By adopting the compression mode of universal material tester to measure young's modulus of hydrophilic fiber-reinforced silica aerogels, the major reason for the large range of deformation is the deformation of the silica aerogel itself. It was recognized that the ultra-low density nanoporous silica micro area deformation can be measured by uniaxial compression mode. (Kucheyv et al). [9] The increase in modulus implies there may be the shrinkage of aerogels, which agrees with the microstructure results.

Fig 6 shows the low-strain springback stress-strain curves obtained through the cycle of thermal shock tests (at room temperature and cryogenic temperature under liquid nitrogen) of hydrophilic fiber-reinforced silica aerogels. 1 to 6 is on behalf of sample after the number of thermal shock in sequence. It's seen from Fig 6 that, when the strain is 0.02 N/mm<sup>2</sup>, the corresponding stress of the sample is 0.041 after the first cycle of thermal shock, and the slope of the stress strain curve is 0.444. While the corresponding stress 0.02 N/mm<sup>2</sup> of sample after the next several cycles is almost lower than 0.0016N/mm<sup>2</sup> and the slope of the stress strain curve is lower than 0.217. Overall, the slope of the stress strain curves exhibit irregular with the cycles of shock. That means in the low-strain modulus of the aerogels decreases but the high-strain modulus increases obviously.

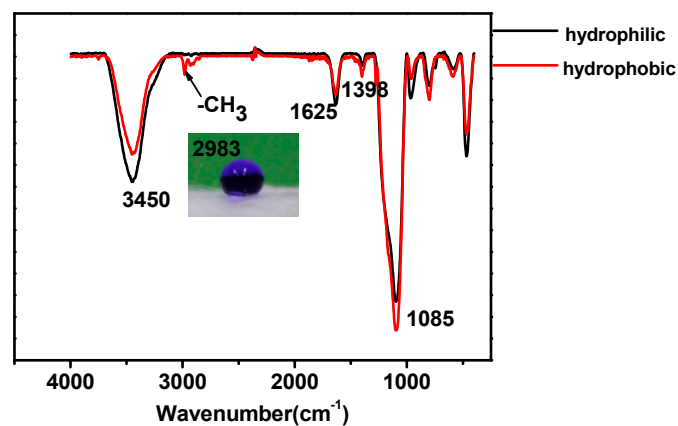


**Figure 7.** FT-IR spectra of the hydrophilic and hydrophobic fiber-reinforced silica aerogels

Fig.7 shows the FT-IR spectra of hydrophilic and hydrophobic aerogels. In Fig.7. The strong peak near  $1085\text{ cm}^{-1}$ , the weak peak near  $800\text{ cm}^{-1}$  and  $464\text{ cm}^{-1}$  were assigned to the asymmetric and symmetric bending vibration of the Si-O-Si bonds. [10] The absorption peaks near  $2983\text{ cm}^{-1}$  and  $2900\text{ cm}^{-1}$  are due to the terminal  $-\text{CH}_3$  groups. And since there are a lot of  $-\text{CH}_3$  group on the sample surface, it will performance hydrophobic characteristics, while there is no peak near  $2983\text{ cm}^{-1}$  and  $2900\text{ cm}^{-1}$  in hydrophilic aerogel.[11]

Fig 7 shows the photographs of water droplets placed on the hydrophobic aerogel, and the corresponding contact angles is  $140^\circ$ . It is notable that the wide band near  $3450\text{ cm}^{-1}$  and the peak at  $1625\text{ cm}^{-1}$  were assigned to the stretching vibration of O-H group and bending vibration of H-O-H, [11-13] indicating that both the hydrophilic and hydrophobic aerogels contain adsorbed water. During the thermal shock process in liquid nitrogen, free water tend to be the ice for the dramatically varied temperature, which may result in the change of the microstructure of the samples.

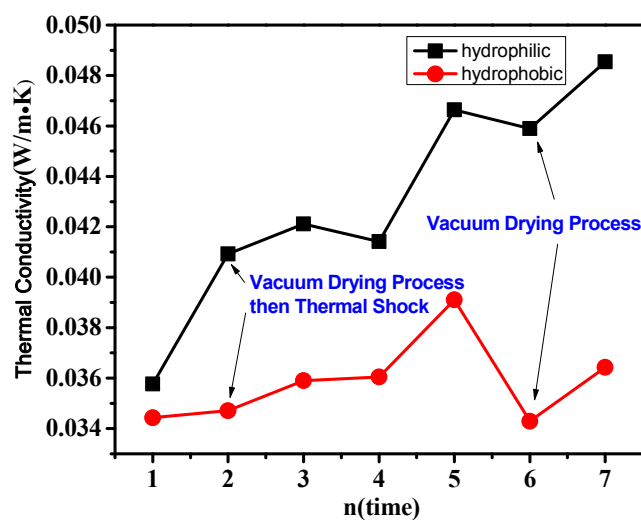


**Figure 8.** Thermal conductivity changing with cycle times with vacuum drying process.

In order to further demonstrate the mechanism, the aerogels were treated at  $80^\circ\text{C}$  under vacuum environment before conducting shock experiments to avoid the effect of the free water. Fig.8 shows that the thermal conductivity of the hydrophilic aerogels increases from  $0.03577\text{ W}/(\text{m}\cdot\text{K})$  to  $0.041\text{ W}/(\text{m}\cdot\text{K})$  while hydrophobic aerogels are increasing from  $0.034\text{ W}/(\text{m}\cdot\text{K})$  to  $0.035\text{ W}/(\text{m}\cdot\text{K})$  after the first shock. Compared to the initial state value, the thermal conductivity of two samples have increased greatly after five cycles, which were  $0.047\text{ W}/(\text{m}\cdot\text{K})$  and  $0.039\text{ W}/(\text{m}\cdot\text{K})$ , respectively.

The aerogels were treated at  $80^\circ\text{C}$  under vacuum environment again (6th Cycle in Fig.8). The thermal conductivity of the hydrophilic aerogel had a small decline from  $0.047\text{ W}/(\text{m}\cdot\text{K})$  to  $0.046\text{ W}/(\text{m}\cdot\text{K})$ , while the thermal conductivity of the hydrophobic aerogel decrease from  $0.039\text{ W}/(\text{m}\cdot\text{K})$  to  $0.034\text{ W}/(\text{m}\cdot\text{K})$ . That indicates the free water in the aerogels may greatly influence the failure behaviors of both hydrophilic and hydrophobic aerogels after thermal shocks.

## 4. Discussion

### 4.1 Thermal conductivity failure process

It was found that the thermal conductivity of hydrophilic aerogel increased by 35.5% after the first shock and kept in a high value, while that of the hydrophobic aerogel increased by 19.5% and kept in a relatively low value after multiple shocks. (Fig.1) The thermal conductivity of samples increased after several cycles of thermal shock. The microstructure of the sample may have changed under the

condition of low temperature. By contrast, after vacuum drying treatment, the hydrophobic aerogels exhibits reversible thermal failure behavior, while the hydrophilic aerogels shows an irreversible behavior. This indicates the driving force of the failure may be due to the adsorbing water.

#### 4.2 Microstructure evolution during the shock processes

Scanning electron microscope (SEM) was used to test samples before and after processing. Compared with the sample before thermal shock, the skeleton becomes thicker and pore size turn into larger for hydrophilic aerogel (Fig.2a and 2b ).While skeleton and pore size of hydrophobic aerogel have barely changed (Fig. 2c and 2d).

Specifically, the specific surface areas reduced by 200 m<sup>2</sup>/g. And peak pore size of the hydrophilic aerogel increased from 18 nm to 25 nm (Sample a and b in table 1.) after thermal shock. Pore size of hydrophilic aerogel become larger and the number of pores decreased in the same volume[14]. It suggests that part of pore was collapsed, which increase the surrounding space. Meanwhile, decrease in specific surface areas may also attributed to destructure of the microstructure after thermal shock, which conforms to the fig.2a and 2b. For hydrophobic aerogel, the specific surface area increases by 100 m<sup>2</sup>/ g, which may be induced by the removal of adsorbed water in the frozen process. And the peak pore size of the hydrophobic aerogel kept at ~9 nm. They indicate that part of pore size of hydrophobic aerogel diminished and part of the big pores reduce to the mesoporous after thermal shock. (Sample c and d in table. 1).In brief, the hydrophilic aerogel suffer more serious from failure process than hydrophobic aerogel.

In the process of studying the failure mechanism, we found hydrophilic and hydrophobic aerogels contain a small amount of water by the FT-IR spectra (Fig.7) and we infer that freezing water caused the volume expansion and resulted in certain damage to the frame during low temperature of thermal shock.

#### 4.3 Supposed failure mechanism of both aerogels during the shock processes

Hydrophobic aerogel suffers less damage because of the unique “Spring-back” effect [15](Fig9a), which is confirmed by SEM images and results of nitrogen adsorption and desorption isotherms. There is obvious shrinkage of frame at first and weak adhesion between skeleton in aerogel under liquid nitrogen. Then the skeleton will be elastically separated. The hydrophobic aerogels after vacuum drying treatment exhibits the spring-back effect (6<sup>th</sup> in Fig8), making the thermal conductivity decrease as low as the untreated samples. On the contrary, hydrophilic aerogel shrink and can't return to its original state. Therefore, we carried on the macroscopic mechanical properties and the mechanical properties of low strain situation for hydrophilic aerogels before and after thermal shock.

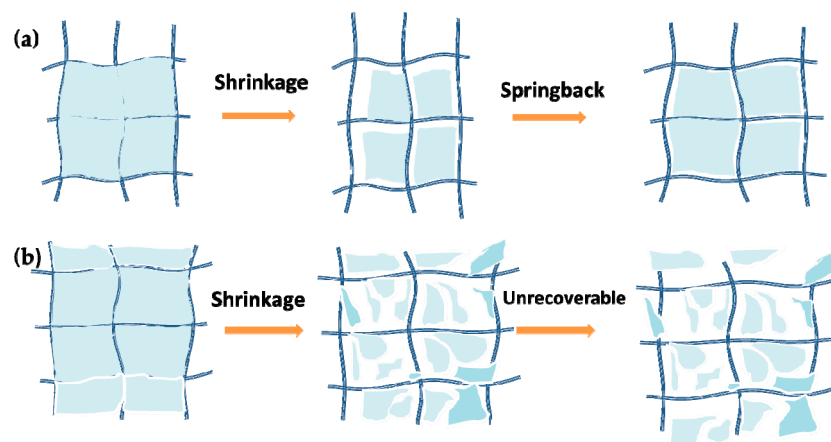


**Figure.9** Schematic diagram about reversible and irreversible process of the hydrophobic (a) and hydrophilic (b) fiber-reinforced silica aerogels

The high-strain hardening and low-strain soften behaviors further demonstrated the skeleton shrinkage of the hydrophilic aerogel. On one hand, as provided in Fig 5, for hydrophilic aerogels, the Young' modulus of sample after thermal shock(2.49 MPa) is 83.09% higher than the slope of sample before thermal shock(1.36 MPa), which means that thermal shock obviously contribute much to the increase in stiffness. The shrinkage increases the density of the aerogels, leading to a large modulus. Also, the thicker skeleton and the larger pore size may make the aerogels rigid when conducting the high-strain compression. On the other hand, it can be seen the slope of the first curve is clearly higher than the other cycles under the low strain (weak stability) in Fig.6. After the first cycle of shock, the young's modulus decreases and loses the regularity. It indicates that silica aerogel shrink, while fiber remains unchanged on account of its stiffness. Because shrinkage of skeleton or external force will make some aerogel on the surface of fiber fall off and fiber-reinforced silica aerogel may separate from the fibers after thermal shock under the low strain (Fig9 b). Therefore, when conducting low-strain compression, only surface fiber is pressed. Lack of the support of the aerogels, the modulus of the samples will decrease naturally.

In order to further demonstrating the mechanism, the aerogels were treated at 80°C under vacuum environment before conducting shock experiments. It indicates that after the first shock, the thermal conductivity of the hydrophilic and hydrophobic aerogels were increased only 14.0% and 0.4% (Fig.8), and the advantages are obvious in comparison with the sample before thermal shock in air. (Fig.1) After 5 cycles of thermal shock, the thermal conductivity of the hydrophilic has little change under the vacuum drying, while the thermal conductivity of hydrophobic aerogels can restored nearly to its original state. They showed that the failure processes of the hydrophilic and hydrophobic aerogels are irreversible and reversible, respectively. (Fig9 a and b)

## 5. Materials and Methods

By the two-step acid-base sol-gel reaction with the fiber composite, combined with supercritical drying, we prepared the hydrophilic and hydrophobic fiber-reinforced silica aerogels.[16] During the thermal shock experiments, at first, hydrophilic and hydrophobic fiber-reinforced silica aerogels are sealed by a plastic bag each other. Company with temperature probe, they were put in a bigger one. Then, they were submerged under liquid nitrogen and start timing after temperature instrument display -196°C for 10 minutes. After 1 hour of low temperature shock, they were removed at room temperature (25°C). Start to test samples after they recovered at room temperature and were kept half an hour. The above process called a cycle. In order to simulate planetary surface environment, we take several cycles.

## 6. Conclusions

As the best thermal insulator, aerogels could be used for high-efficiency insulation under exoplanet environment. Under the condition of low temperature, residues such as numerous hydroxyls in the surface and water in the fiber-reinforced silica aerogels will damage its structure and thermal property. The hydrophobic aerogels exhibits a spring back behavior, thus its failure process is reversible. Therefore, for the space exploration, it is necessary to use the aerogel with hydrophobic surface. Despite the water content in the exoplanet environment (such as the Mars) is very few, the adsorbing water cannot be avoided during the storage in the ground. Therefore when planning to use the aerogels, it is necessary to conduct vacuum drying treatment in order to reduce the damage or the failure during the shock processes.

## Acknowledgements

We are thankful for financial support from Bayer-Tongji Eco-Construction & Material Academy. National High Technology R&D Program of China (2013AA031801), National Natural Science Foundation of China (51172163), Science and Technology Innovation Fund of Shanghai Aerospace, China (SAST201321).

## References

1. Du, A., et al., A special material or a new state of matter: a review and reconsideration of the aerogel. *Materials* **2013**, *6*, 941-968.
2. Fesmire, J. and J. Sass, Aerogel insulation applications for liquid hydrogen launch vehicle tanks. *Cryogenics* **2008**, *48*, 223-231.
3. Gurav, J.L., et al., Silica Aerogel: Synthesis and Applications. *J. Nanomaterials* **2010**, *2010*, 1-11.
4. Bheekhun, N., A.R. Abu Talib, and M.R. Hassan, Aerogels in Aerospace: An Overview. *Adv. Materials Sci. Engineer.* **2013**, *2013*, 1-18.
5. Trevino, L.A. and E.S. Orndoff, Advanced space suit insulation feasibility study. 2000.
6. Paul, H.L. and K.R. Diller, Comparison of thermal insulation performance of fibrous materials for the advanced space suit. *J. Biomechanical Engineer.* **2003**, *125*, 639-647.
7. Zhao, S., et al., Multiscale Assembly of Superinsulating Silica Aerogels Within Silylated Nanocellulosic Scaffolds: Improved Mechanical Properties Promoted by Nanoscale Chemical Compatibilization. *Adv. Functional Materials* **2015**, *25*, 2326-2334.
8. Schwan, M. and L. Ratke, Flexibilisation of resorcinol-formaldehyde aerogels. *J. Materials Chem. A* **2013**, *1*, 13462.
9. Kucheyev, S.O., et al., Super-compressibility of ultralow-density nanoporous silica. *Adv. Mater.* **2012**, *24*, 776-80.
10. Lee, S., et al., The effect of pH on the physicochemical properties of silica aerogels prepared by an ambient pressure drying method. *Materials Letters* **2007**, *61*, 3130-3133.
11. Bhagat, S.D. and A.V. Rao, Surface chemical modification of TEOS based silica aerogels synthesized by two step (acid-base) sol-gel process. *Applied Surface Science* **2006**, *252*, 4289-4297.
12. Venkateswara Rao, A., N.D. Hegde, and P.M. Shewale, Imperviousness of the hydrophobic silica aerogels against various solvents and acids. *Applied Surface Science* **2007**, *253*, 4137-4141.
13. Folgar, C., et al., Microstructural evolution in silica aerogel. *J. Non-Crystalline Solids* **2007**, *353*, 1483-1490.
14. Bangi, U.K.H., A. Venkateswara Rao, and A. Parvathy Rao, A new route for preparation of sodium-silicate-based hydrophobic silica aerogels via ambient-pressure drying. *Sci. Technol. Adv. Mater.* **2016**, *9*, 035006.
15. Hwang, S.-W., et al., Effective preparation of crack-free silica aerogels via ambient drying. *J. Sol-Gel Sci. Technol.* **2007**, *41*, 139-146.
16. Deng, Z., et al., High strength SiO<sub>2</sub> aerogel insulation. *J. Non-Crystalline Solids* **1998**, *225*, 101-104.

